

Fully sealed metal nanoparticle film based field-effect transistor

Yuxue Cai

Institute of Physical Chemistry, University of Hamburg, 20146 Hamburg, Germany

Jan Michels

*Physics and Chemistry Departments, Interdisciplinary Nanoscience Center Hamburg,
University of Hamburg, Sedanstrasse 19, 20146 Hamburg, Germany*

Julien Bachmann

*Physics and Chemistry Departments, Interdisciplinary Nanoscience Center Hamburg,
University of Hamburg, Sedanstrasse 19, 20146 Hamburg, Germany and
Chemistry Department, University of Erlangen-Nurnberg, Egerlandstrasse 3, 91058 Erlangen, Germany*

Christian Klinke*

Institute of Physical Chemistry, University of Hamburg, 20146 Hamburg, Germany

Devices comprising one or a few small conductive islands show a rich spectrum of electrical behavior attributed to the effect of Coulomb blockade. We demonstrate that in extended, monolayered films assembled from individual, monodisperse metal nanoparticles current oscillations can be observed using a local top gate realizing transistor function. A property analogous to the bandgap of semiconductors is attained in this metal-based system by the Coulomb energy gap which is tunable via the nanoparticle size. These metal nanoparticle field-effect transistors are easy to prepare and stable for months due to a protecting oxide layer.

Introduction

Devices founded on new principles, promising new functions, higher performance, or reduction of production costs should anyhow be reliable, large-scale producible, and CMOS compatible [1]. One branch of material synthesis which can fulfill these requirements is colloidal chemistry [2]. The introduction of colloidal chemistry to the synthesis of inorganic nanoparticles has caused a tremendous development of the field in the recent decades [3]. Today, the control over nucleation and growth phases allows controlling the crystal size, while the amount and nature of ligand molecules and precursors permits control over shape, surface properties, and atomic composition of the nanoparticles [4]. In some systems it is possible to synthesize such structures with almost atomic precision and in macroscopic amounts by colloidal chemistry; such structures are then called nanoparticles [3, 5]. The colloidal synthesis of nanoparticles is comparatively fast, inexpensive, and scalable. This enables one to spread nanoparticles easily and homogeneously by e.g. spin-coating onto flat surfaces such as silicon or silicon oxide [6]. One method which is able to generate monolayered highly ordered films over vast areas is the Langmuir-Blodgett (LB) method [7]. This delivers an experimental access to the percolative transport through such films [8, 9]. Beside others, our group has extended the method for high quality films and investigated the electrical properties of such films [7, 10, 11]. Combined with microcon-

tact printing the Langmuir-Blodgett technique has been utilized previously to assemble structured monolayers of nanoparticles in two-dimensional Au, Pt/Fe₂O₃, and Co patterns [12–14]. The standard LB technique implies the film preparation by deposition of the particles onto water as sub-phase. The problem is that nanoparticles with a hydrophobic organic ligand shell which stabilizes them in organic solvents often tend to agglomerate on water, whereas on standard organic solvents they sink. In a new approach our group deposited nanoparticles onto diethylene glycol as subphase with an intermediate polarizability [7, 10, 11]. This methodology yields highly ordered metal nanoparticle films over unprecedented vast areas in the micrometer up to the centimeter range.

For a long time, scientists have been interested in the properties of items composed of a few atoms, called quantum dots [15–17]. The electrical transport properties of these confined systems have been studied for quite some time [18–20]. Such simple devices allow for the verification of theoretical models and a vast number of experimental and theoretical results have been published dealing with the transport through nanoparticle arrays [21–25]. The tunable character of the superstructures makes them interesting model systems for charge transport studies in confined systems [26]. The transport has been described by various theories [16, 27–29]. Researchers have also observed that in such films charging effects occur attributed to Coulomb blockade [30–32].

Quantum dots (or nanoparticles) in which the electrons are confined in all three dimensions can be considered as zero-dimensional. Due to their small size they also possess a small electrical capacity. This in turn, leads to a relatively high charging energy ($E_C = e_o^2/2C$) necessary to tunnel one electron onto this conductive island.

*Electronic address: klinke@chemie.uni-hamburg.de

At low temperatures and small bias voltages the thermal energy of the electrons is not sufficient to overcome the charging energy. At higher voltages the energy for electrical transport through the quantum dot is delivered by the applied electrical field. This phenomenon is known as *Coulomb blockade*. We already demonstrated that colloidal nanoparticle films are subjected to Coulomb blockade at low temperature [10, 11]. The blockade regime can be overcome by higher voltages where electrons start to tunnel from nanoparticle to nanoparticle, or by higher temperatures where thermally activated hopping overcomes the blockade. The introduction of a third electrode leads to three-terminal devices which act as *single electron transistors*. For individual nanostructures this was demonstrated in the late 80s by Fulton and Dolan [33]; later also for one [34] or a few [35] individual nanoparticles. A nice overview about the foundations, prospects, and applications in the field of single-electron devices can be found in the review by Likharev [36].

In a regular crystal with atoms as constituents the electronic behavior is mainly determined by the energy levels of the atoms, the coupling between adjacent sites, and the symmetry of the solid. These properties are not free to choose but given by nature. In "artificial atoms" like the nanoparticles it is possible to control these properties by the used material (work function), by the size and shape of the nanoparticles, by the coupling determined by the organic ligands, and by their assembly. For example, a decrease of the distance between adjacent nanoparticles increases the coupling between them and leads to a decrease of the Coulomb charging energy of the individual conductive islands. Eventually, this leads to a transition from insulating to metallic behavior (Mott-Hubbard transition) [37]. Often the I-V curves of granular films can be fitted with the equation of Middleton and Wingreen [15] $I(V) = A((V - V_T)/V_T)^\zeta$. The threshold voltage V_T and the exponent ζ depend on the dimensionality of the film. The non-linear increase in conductivity above the threshold voltage $V > V_T$ is attributed to the opening of conduction paths in the film. For roughly two-dimensional films the value for ζ has been found experimentally to be about 2.25 and for fractal films to be around 4.12 [38–40]. In theoretical considerations values of $\zeta = 1$ has been predicted for one-dimensional structures such as chains of nanoparticles and a value of $\zeta = 5/3$ for two-dimensional films [15].

Conventional transistors are based on semiconductor materials. The electrical conduction through metallic multi-tunnel devices is extraordinarily interesting since they could serve as conducting layer in new or improved inexpensive electronic devices. The Coulomb energy (due to charging of the ultra-small capacity of the nanoparticles) takes over the role of the bandgap in a semiconductor. Thus, it is desirable to keep the nanoparticles individualized (a merging of the particles would render the films metallic again).

So far, it has not been possible to directly demonstrate the Coulomb blockade (oscillations) in nanoparticle films

by application of a third electrode, the gate electrode, which defines the electrical potential at the position of the conducting channel (and thus the current across it) without directly contacting it. The idea is to exploit the fact that the conduction electrons on the nanoparticles in a monolayer film cannot be screened efficiently and thus be influenced by a gate electrode.

We demonstrate that in monolayered films of well-organized metal nanoparticles current oscillations can be observed using a local top gate realizing transistor function. Instead of the semiconductor band gap, the physical basis of the device is the Coulomb energy gap, a property which is tunable by the nanoparticle size. We attribute the success to the high quality of the nanoparticles, the monolayer film, and the atomic layer deposition (ALD) oxide that we used as gate dielectric.

Synthesis and assembly

We chose a synthesis for cobalt-platinum nanoparticles under Schlenk conditions which was published by Shevchenko et al. [41] and successfully applied in previous experiments [7, 10, 11]. It produces monodisperse nanoparticles with high chemical stability. We synthesized nanoparticles in two different sizes and shapes. The spherical nanoparticles have a diameter of 7.6 ± 0.5 nm and the cubic nanoparticles have 9.3 ± 0.8 nm. The particles were analyzed by energy dispersive X-ray analysis (EDX) to have a composition of $\text{Co}_{0.20}\text{Pt}_{0.80}$.

The nanoparticles were synthesized by simultaneous reduction of platinum acetylacetonate ($\text{Pt}(\text{acac})_2$) and thermal decomposition of cobalt carbonyl ($\text{Co}_2(\text{CO})_8$) in the presence of 1-adamantane carboxylic acid (ACA) and hexadecylamine (HDA) as stabilizing agents. In a standard procedure, 65.6 mg $\text{Pt}(\text{acac})_2$ was dissolved in 8 g HDA, 0.496 g ACA, 0.26 g 1,2-hexadecanediol (HDD) and 4 mL diphenylether at 65°C . When the solution turned clear, the mixture was degassed three times and heated to the injection temperature (165°C for the spherical and 155°C for the cubic nanoparticles). 92 mg $\text{Co}_2(\text{CO})_8$ dissolved in 1.6 mL 1,2-dichlorobenzene were separately degassed three times at room temperature and injected quickly into the mixture under vigorous stirring. After stirring for one hour at the injection temperature, the temperature was increased to 230°C for two additional hours. The obtained particles were precipitated with 2-propanol, centrifuged, and re-suspended in toluene.

Figure S1 (see Supporting Information) shows a zoom series of TEM pictures of monodisperse spherical nanoparticles. The cobalt-platinum nanoparticles formed highly ordered monolayer films, wherein the particles were arranged in hexagonal domains. The quality of the nanoparticles has also been checked by XRD. Figure S2 (see Supporting Information) shows a diffractogram of the spherical and the cubic nanoparticles. There are almost no differences between the two diffractograms,

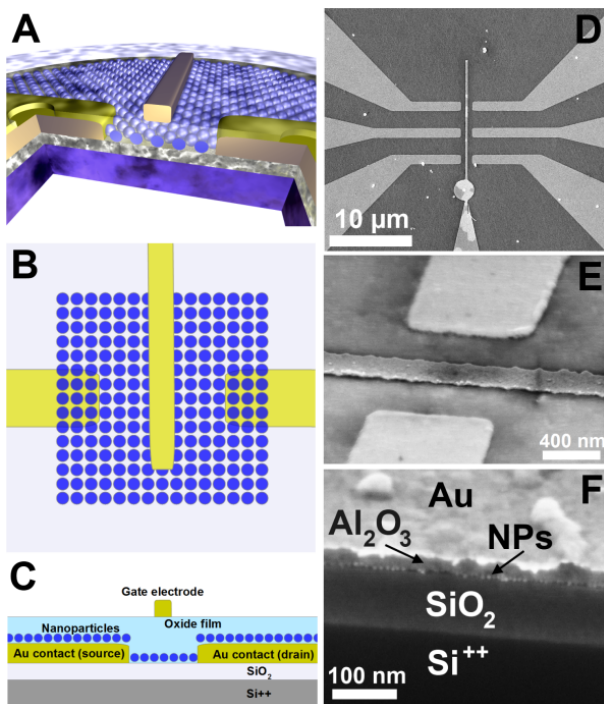


FIG. 1: *Structure of the Coulomb blockade based transistor.* (A) 3D sketch of the device (Not to scale!); (B) Top view; (C) Cross-section sketch; (D) Top view SEM image: From left and right the gold electrodes are entering the view and defining three parallel devices. In the center the vertical structure is the top gate electrode on the ALD Al_2O_3 film (perpendicular to the charge flow) which has no contact to the nanoparticle film; (E) Closed, tilted view: The top gate electrode is clearly visible. The contacts are a bit blurred since they are located below the ALD film which is semi-transparent to the electron-beam; (F) Cross-sectional SEM image at the top gate position showing all important components of the device.

showing that the spherical and cubic nanoparticles have the same composition.

Classically, spin- and dip-coating [42] are used to prepare films of nanoparticles. Those methods are usually not suitable for high quality monolayers of nanoparticles. Thus, we developed an approach to prepare 2D structures based on the Langmuir-Blodgett method. We modified this technique in order to be able to deposit nanoparticle films over vast areas in highest quality. For the monolayer preparation the nanoparticles were washed two more times, re-suspended in toluene and spread onto the diethylene glycol subphase. After the toluene was evaporated, the nanoparticles were compressed by the barrier with a speed of 2 mm/min to a target pressure of 10 mN/m. The monolayer film was held at the target pressure for about two hours, allowing the film to relax and to rearrange. The high quality of the monolayers can be seen in Figure S1 (Supporting Information). The monolayer film was then deposited onto the surface of a Si/SiO₂-wafer (with 300 nm oxide) which was structured

with gold electrodes (1000 nm width, 1200 nm inter-electrode distance) by e-beam lithography. On top of this structure we deposited the nanoparticle film by the Langmuir-Blodgett method. Subsequently, we deposited different thicknesses (55 nm, 77 nm, and 150 nm) of aluminum oxide layer by atomic layer deposition (ALD); and on top of the aluminum oxide we performed an additional e-beam lithography step in order to define a top gate electrode precisely between the lateral contacts. The whole ensemble works as three-terminal device, a field-effect transistor. The top gate, in contrast to a bottom gate, allows for a more precise electrostatic control of the nanoparticle film. The device concept is shown in Figure 1A-C. The real device was imaged by scanning electron microscopy and is displayed in Figure 1D-E. The lateral electrodes in Figure 1E are somewhat fuzzy since they are underneath the aluminum oxide layer, which is semi-transparent to the electron-beam. In Figure 1F a cross-section is displayed. It nicely shows the assembly of silicon oxide on highly-doped silicon, then the important monolayer of metal nanoparticles, the ALD film and finally the top electrode.

Atomic layer deposition (ALD) is a technique for the deposition of thin solid layers from the gas phase characterized by low processing temperatures and conformal coatings of structured substrates [44, 45]. Amongst others, metal oxide depositions using ALD have been very well studied. Here, two precursor gases are used in alternating manner, an organometallic metal-containing complex and a reagent that provides oxygen - in the case of aluminum oxide, trimethylaluminum (TMA) and water are typically used. First, the metal alkyl reacts with the hydroxyl-terminated surface. In the second step, water hydrolyses the adsorbed metal alkyls to regenerate a new layer of hydroxide groups for the next TMA pulse. Since each step is a self-limiting surface reaction, the whole procedure can be carried out in an excess of the precursor gases and the growth rate is independent of exact precursor amounts.

The Al_2O_3 films were created by atomic layer deposition (ALD) from trimethylaluminum (TMA) and water in a self-made ALD reactor using nitrogen as carrier gas. TMA was kept at room temperature, water at 40 °C, and the samples were heated to 100 °C. Each ALD cycle consisted of the following sequence: TMA pulse (0.1 s), exposure (20 s), purge (40 s), then water pulse (0.5 s), exposure (20 s), and purge (40 s). In these conditions, 546 ALD cycles correspond to approximately 77 nm of Al_2O_3 , respectively. The thickness of the ALD layers was measured with a variable-angle spectroscopic ellipsometer by Dr. Riss Ellipsometerbau GmbH.

Electrical characterization

In order to characterize the properties of the constructed devices several electrical measurements have been performed. First, the devices have been evalu-

ated by 2-point measurements. The conductance curves dI_D/dV_{DS} vs. V_{DS} in Figure 2 show clearly that for spherical nanoparticles and temperatures below 10 K the film is in Coulomb blockade at biases below about 1.5 V (the corresponding IDS-VD curves are shown in Figure S3 in the Supporting Information). At higher temperatures the Coulomb blockade bias is reduced and at temperatures over 20 K it is completely lifted. Using the larger cubic nanoparticles the Coulomb blockade bias lies roughly at 0.5 V at 4.3 K. This is due to the lower activation energy for tunneling across the gaps between the cubic nanoparticles, in accordance with our earlier publication [11].

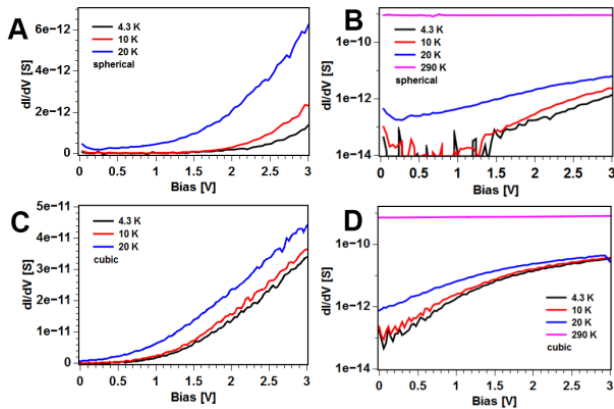


FIG. 2: **2-point measurements.** In (A) the conductivity dI_D/dV_{DS} of a film using spherical nanoparticles is shown. At low temperatures the film is in Coulomb blockade which can better be seen in (B) which shows the same data on a log-scale. (C) shows the data for a film using cubic nanoparticles. (D) shows the data on a log-scale. Signs of Coulomb blockade are difficult to recognize. Both films are covered with 77 nm Al_2O_3 .

The corresponding current-voltage curves can be fitted with the threshold voltage model from Middleton et al. [15]. We fit the current-voltage curves of spherical and cubic nanoparticles measured at 4.3 K and determine the ζ values and the threshold voltages (see Figure S4 in the Supporting Information). For the spherical nanoparticles we obtain a ζ value of about 3.0 and a threshold voltage of 1.6 V. The cubic nanoparticles show a threshold voltage at 0.6 V and we obtain a ζ value of 2.6. The different ζ values of the two different particle shapes are probably caused by the different packing of the film. The deviation in the threshold voltages is caused by the different Coulomb energies of the nanoparticles [11]. The ζ values are much higher than theory predicts [15] but in agreement with the experimental values from other groups [46–48]. For metallic 2D nanoparticle arrays ζ values of 2 to 2.5 were determined, depending on the size distribution of the nanoparticles. For multilayer nanoparticle films ζ values of about 2.6 to 3 were determined [21, 46–48]. Gold nanoparticle arrays with strong topological inhomogeneities show ζ values of about 4 [49].

Calculations and experimental results suggest that

the charging energy only depends on the particles' self-capacitance (C_{self}) and is almost independent of the interparticle distance [11]. Thus, the charging energy is independent of the geometric capacitance, as well. This was demonstrated by calculations using the finite-element method. The geometrical capacitance starts to be predominant over the self-capacitance when the particles' diameter exceeds one micrometer. Therefore, the charging energy of smaller particles only depends on the dielectric constant (ϵ_r) of the interparticle medium and on the particles' radius. The dielectric constant of the interparticle medium was calculated by using the activation energy:

$$E_a = \frac{e^2}{2C_{\text{self}}} = \frac{e^2}{8\pi\epsilon_o\epsilon_r R} \Leftrightarrow \epsilon_r = \frac{e^2}{8\pi\epsilon_o R E_a}$$

The activation energy is deduced from the slope of a corresponding Arrhenius plot. For spherical nanoparticle of 7.6 nm in diameter an activation energy of 20 meV and a dielectric constant of 9.5 was calculated. The self-capacitance of the spherical particle is thus 4.0 aF. These values are on the same order of magnitude as the values of earlier publications [11, 47].

Further, we measured the lateral current I_D through the nanoparticle films with a layer of 77 nm Al_2O_3 as a function of the top gate electrode V_{tg} from -4 V to 4 V (or from 0 V to 8 V) while stepping the bias V_D from -3 V to 3 V in 0.5 V steps. Figure 3 shows on the left side (A, C, E) the relative change of the current and on the right side (B, D, F) the absolute change. The relative change of the current is defined by $I_D \text{ rel.} = I_D/I_{D,0}$ using the last values of the current in the measured range $I_{D,0}$. The absolute change of current is defined by $I_D \text{ abs.} = I_D - I_{D,0}$. Those current variations are defined in order to increase the visibility of the effects. In the relative current plots the changes are more clearly seen for small biases, and in the absolute current plots the changes for larger biases are more obvious. At 4.3 K, the film using spherical nanoparticles shows Coulomb oscillations at a bias of 2.0 V and above. With cubic nanoparticles the Coulomb oscillations are already visible at a bias of 1.0 V. These values are in agreement with the values of the threshold voltage and the Coulomb blockade values from the current-voltage curves. The peaks of the Coulomb oscillations are non-periodic, in accordance with the sequential tunneling of the charge through multiple particles and pathways [50]. In relative terms, the Coulomb oscillations can be seen most clearly just above the threshold voltage, because under these conditions the electrical field is sufficient to overcome the Coulomb blockade through the whole film for the first time and the charge transport most probably takes place along a single path or a small number of branches. If the voltage is increased, then the current flows through multiple pathways, which branch out and reconnect [15], and the Coulomb oscillations become weaker. In absolute value, the oscillations are more pronounced for higher biases due to an overall higher current. The raw data for

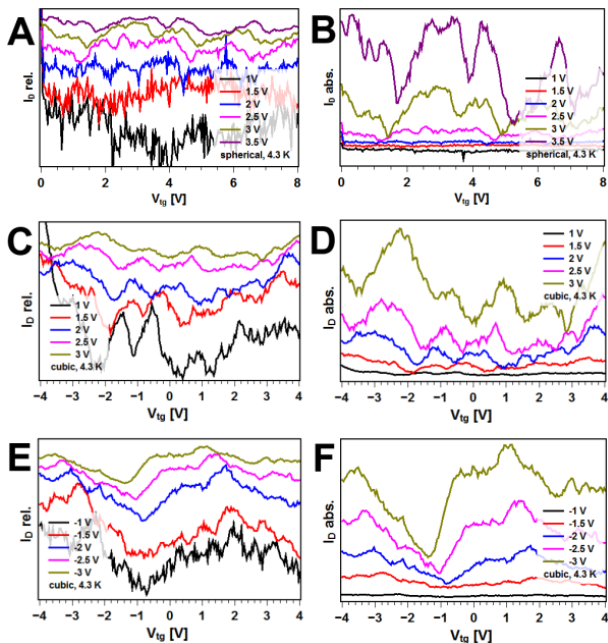


FIG. 3: *3-point measurements as a function of bias.* Lateral current I_D as a function of the applied top-gate voltage V_{tg} . For spherical nanoparticles (smaller size, larger Coulomb charging energy) the oscillations start at a bias of about 2.0 V at 4.3 K (A). For the cubic nanoparticles Coulomb oscillations are already visible at a bias of 1.0 V (C, E). On the left side the relative changes $I_D/I_{D,0}$ are shown (A, C, E) and on the right side the absolute changed $I_D - I_{D,0}$ (B, D, F). For clarity the curves are shifted on the y-scale. In the latter the changes are clear to see not because the relative change is larger but the absolute value of the current is larger at larger biases. The relative current change is larger for smaller value of the bias voltage V_{DS} . All measured films are covered with 77 nm Al_2O_3 . For better visibility the curves are stacked. Thus, we do not show scales here but in Figure 5.

the source, drain, and top gate current are exemplarily shown for a bias of -3 V in Figure S5 in the Supporting Information.

In order to better understand the electrostatic properties of the devices we performed simulations using the finite element method. Figure 4 shows in (A) the distribution of the electric potential at 1.0 V bias and 0.5 V top gate voltage and in (B) the potential along the conductive path is shown for different top gate voltages. It turns out that the local electrical potential and the electrical field can nicely be tuned by a local top gate. We attribute the oscillations in the $I_D - V_{tg}$ curves to a change in the local electrical potential. With the change of the electrical potential, the gate voltage where the oscillations are their minimum or maximum is changed, too.

The features in the curves shift to more positive gate voltages with increasing positive bias and to more negative gate voltages with increasing negative bias, which is in accordance with the picture of sequential tunnelling through multiple particles. At the half value of the bias

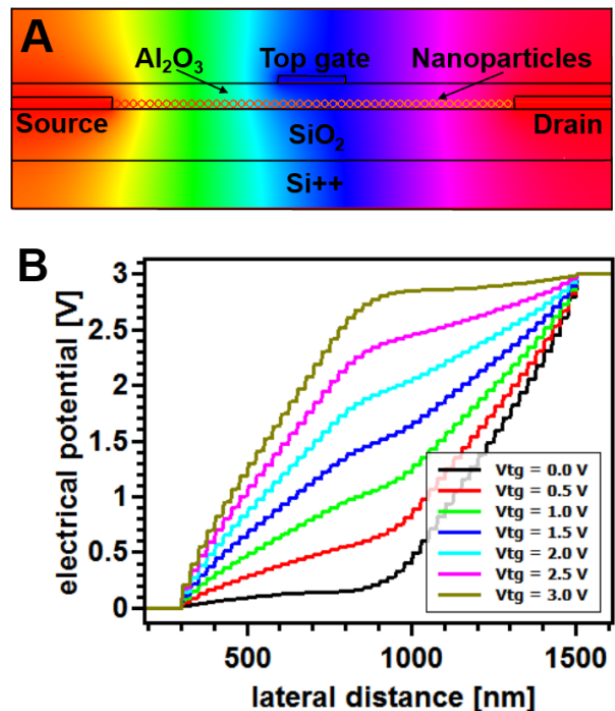


FIG. 4: *Finite element method simulations of the electrical potential of the metal nanoparticle transistor.* (A) Cross-section through the device at 1.0 V drain voltage and 0.5 V gate voltage. Red corresponds to a potential of 0.0 V and pink to 1.0 V. (B) Potential along the path of conduction from the left to the right electrode. The left electrode (source) is at 0.0 V and the right one (drain) at 1.0 V. The top gate voltage is tuned stepwise from 0.0 V to 1.0 V. The backgate (Si^{++}) is left floating. In the spherical particles the potential is constant leading to stepped functions.

the curves always show a local minimum $V_{tg} = V_{DS}/2$. This is because at this top gate voltage the maximum occurring electrical field strength has a minimum.

For the temperature measurements we also swept the top gate electrode voltage V_{tg} from -4 V to 4 V (or from 0 V to 8 V). Exemplarily, we show the curves at a bias of 3 V. With increasing measurement temperature the Coulomb oscillation become weaker as shown in Figure 5. At 50 K the oscillations vanish altogether. At elevated temperature, conductance through the nanoparticle films is no longer determined by the Coulomb blockade. In absolute terms, the oscillations become more pronounced with increasing temperature due to a higher current level, but also vanish at 50 K. The maximum temperature where Coulomb oscillations can be observed is 20 K. This is in accordance with the values from the $I_D - V_{DS}$ curves. Above 20 K the Coulomb oscillations are completely lifted. Figure 5A shows also that the modulation of the lateral current by the top gate is on the order of $\pm 5\%$.

We also characterized samples with three different Al_2O_3 layer thicknesses of 55 nm, 77 nm, and 150 nm. The Al_2O_3 layer should be as thin as possible to ensure

the strongest effect of the top gate, but be thick enough to prevent leakage current in the top gate. The minimum and maximum layer thicknesses must be determined experimentally. For the measurement again we sweep the top gate voltage from -4 V to 4 V and set the bias from ± 1 V to ± 3 V. Exemplarily, we show the curves at -2 V because the curves at this voltage are least noisy. With increasing layer thickness the Coulomb oscillations become weaker and the oscillation frequencies decrease. It can be seen most clearly in the absolute change plots as shown in Figure 6. With 55 nm and 77 nm Al_2O_3 , Coulomb oscillations are clearly visible in the current plots. The Coulomb oscillations of the film with 150 nm Al_2O_3 becomes noisy in the relative plot and is not observable at all in at the absolute plot. The thinner the oxide layer is, the more pronounced are the features in the plots, but with decreasing oxide layer the gate leakage current increased. The variation of the oxide layer thickness provides an ideal Al_2O_3 thickness of 77 nm. At this thickness the oscillations are clearly visible and the leakage current is within the noise level of the setup of 10^{-14} A. With 55 nm Al_2O_3 , the oscillations are more precisely defined and the oscillation frequencies are higher, since the gate electrode is closer to the film, so that the local potential at the particles is influenced more directly, but with the smaller distance from the gate electrode to the film a small leakage current is partially measurable. For larger oxide layers the leakage currents are smaller than the noise level. With 150 nm Al_2O_3 the distance to the film is too large, so that the effect of the gate is barely measurable.

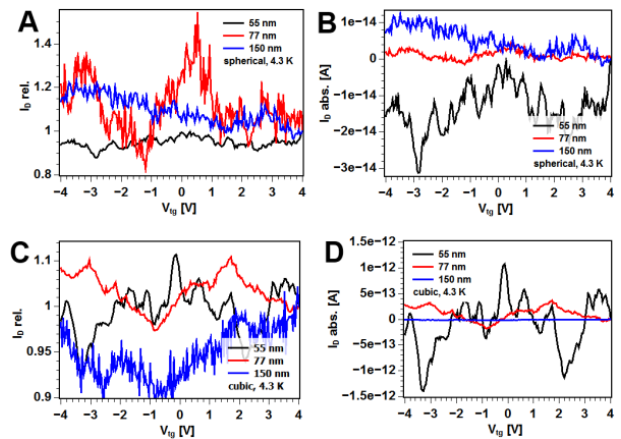


FIG. 6: *3-point measurements as a function of gate oxide thickness.* Lateral current I_D as a function of the Al_2O_3 layer thickness at a bias of -2 V with spherical (A, B) and (C, D) cubic nanoparticles. With 55 nm and 77 nm of Al_2O_3 the oscillation is clearly visible. With 150 nm of Al_2O_3 the oscillation becomes noisy in the relative change and is not to see in the absolute change.

in finite element simulations. They show that the highest field along the path through the nanoparticles under the top gate decreases sharply with increasing distance (Figure S6).

Conclusion

To conclude, the electrical measurements conducted in this work showed, for the first time, that a Coulomb blockade based transistor using a two-dimensional colloidal metallic nanoparticle film is possible. For that, we used well-separated, well-organized nanoparticles in order to maintain the Coulomb blockade features of individual nanoparticles. Anyhow, the fixed distance of about 1 nm allows for an overlap of the wave function to enable tunneling. Thus, Coulomb oscillations were observed in the current vs. top gate voltage plots. With increasing measurement temperature, the oscillations weaken and disappear at above 20 K. It was also found that with increasing distance between the top gate electrode and the nanoparticle film, the effect of the top gate electrode decreased. A change of bias led to a shift of the oscillation peaks. This was attributed to a change of the local electric potential. The low temperature current-voltage curves were fitted with the equation of Middleton and Wingreen [15]. The adjustments provided for spherical and cubic particles ζ values of 3.0 and 2.6 and threshold voltages of 1.6 V and 0.6 V in good agreement with the values of similar metallic films from other groups [21, 46, 48]. The prepared nanoparticle film devices using different batches of synthesized nanoparticles, with different particle shapes and sizes behave very reliably and according to theory. They are stable over time due to the protective oxide layer which is the top gate dielec-

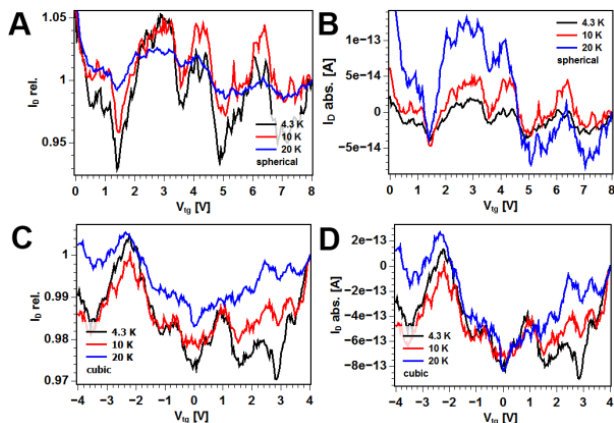


FIG. 5: *3-point measurements as a function of temperature.* Lateral current I_D as a function of temperature at a bias of 3.0 V with spherical (A, B) and cubic (C, D) nanoparticle films (both covered with 77 nm Al_2O_3). (A, C) relative change $I_D/I_{D,0}$; (B, D) absolute change $I_D - I_{D,0}$. The relative changes become weaker with increasing temperature and vanish at 50 K. This is more pronounced for the smaller particles. The absolute changes become more pronounced with increasing temperature. This is due to an overall increase of the current with temperature.

The effect of top gate distance could also be observed

tric. The processing of the metal nanoparticle transistor is simple, inexpensive, and CMOS compatible, whereas the particular transfer characteristics can lead to appli-

cations exhibiting new functionality. For the future, it should be possible to increase the temperature of operation by the use of smaller nanoparticles.

-
- [1] Tao, A. R.; Huang, J.; Yang, P., Langmuir-Blodgett of Nanocrystals and Nanowires. *Acc. Chem. Res.* 2008, 41, 1662-1673.
- [2] Weller, H., Synthesis and self-assembly of colloidal nanoparticles. *Phil. Trans. R. Soc. A* 2003, 361, 229-240.
- [3] Park, J.; Joo, J.; Kwon, S. G.; Jang, Y.; Hyeon, T., Synthesis of Monodisperse Spherical Nanocrystals. *Angew. Chem. Int. Ed.* 2007, 46, 4630-4660.
- [4] Ahrenstorf, K.; Albrecht, O.; Heller, H.; Kornowski, A.; Gorklitz, D.; Weller, H., Colloidal Synthesis of Ni_xPt_{1-x} Nanoparticles with Tuneable Composition and Size. *Small* 2007, 3, 271-274.
- [5] Shevchenko, E. V.; Talapin, D. V.; Schnablegger, H.; Kornowski, A.; Festin, O.; Svedlindh, P.; Haase, M.; Weller, H., Study of Nucleation and Growth in the Organometallic Synthesis of Magnetic Alloy Nanocrystals: The Role of Nucleation Rate in Size Control of CoPt₃ Nanocrystals. *J. Am. Chem. Soc.* 2003, 125 9090-9101
- [6] Malynych, S.; Luzinov, I.; Chumanov, G., Poly(Vinyl Pyridine) as a Universal Surface Modifier for Immobilization of Nanoparticles. *J. Phys. Chem. B* 2002, 106, 1280-1285.
- [7] Aleksandrovic, V.; Greshnykh, D.; Randjelovic, I.; Fromsdorf, A.; Kornowski, A.; Roth, S. V.; Klinke, C.; Weller, H., Preparation and Electrical Properties of Cobalt-Platinum Nanoparticle Monolayers Deposited by the Langmuir-Blodgett Technique. *ACS Nano* 2008, 2, 1123-1130.
- [8] Arai, T.; Saito, S.; Fukuda, H.; Onai, T., Synthesis, Monolayer Formation, and Control of Electrical Characteristics of 3-nm-Diameter Gold Nanoparticles. *Jpn. J. Appl. Phys.* 2005, 44, 5667.
- [9] Hosoki, K.; Tayagaki, T.; Yamamoto, S.; Matsuda, K.; Kanemitsu, Y., Direct and Stepwise Energy Transfer from Excitons to Plasmons in Close-Packed Metal and Semiconductor Nanoparticle Monolayer Films. *Phys. Rev. Lett.* 2008, 100, 207404.
- [10] Cai, Y.; Wolfkuhler, D.; Myalitsin, A.; Perlich, J.; Meyer, A.; Klinke, C., Tunable Electrical Transport through Annealed Monolayers of Monodisperse Cobalt-Platinum Nanoparticles. *ACS Nano* 2010, 5, 67-72.
- [11] Greshnykh, D.; Fromsdorf, A.; Weller, H.; Klinke, C., On the Electric Conductivity of Highly Ordered Monolayers of Monodisperse Metal Nanoparticles. *Nano Letters* 2008, 9, 473-478.
- [12] Tanaka, H.; Mitsuishi, M.; Miyashita, T., Tailored-Control of Gold Nanoparticle Adsorption onto Polymer Nanosheets. *Langmuir* 2003, 19, 3103-3105.
- [13] Guo, Q.; Teng, X.; Yang, H., Fabrication of Magnetic FePt Patterns from Langmuir-Blodgett Films of Platinum-Iron Oxide Core-Shell Nanoparticles. *Adv. Mater.* 2004, 16, 1337-1341.
- [14] Park, J.; Lee, W.; Bae, S.; Kim, Y. J.; Yoo, K.; Cheon, J.; Kim, S., Langmuir Monolayers of Co Nanoparticles and Their Patterning by Microcontact Printing. *J. Phys. Chem. B* 2005, 109, 13119-13123.
- [15] Middleton, A. A.; Wingreen, N. S., Collective transport in arrays of small metallic dots. *Phys. Rev. Lett.* 1993, 71, 3198-3201.
- [16] Averin, D. V.; Likharev, K. K., Coulomb blockade of single-electron tunneling, and coherent oscillations in small tunnel junctions. *J. Low Tem. Phys.* 1986, 62, 345-373.
- [17] Bezryadin, A.; Dekker, C.; Schmid, G., Electrostatic trapping of single conducting nanoparticles between nanoelectrodes. *Appl. Phys. Lett.* 1997, 71, 1273-1275.
- [18] Sampaio, J. F.; Beverly, K. C.; Heath, J. R., DC Transport in Self-Assembled 2D Layers of Ag Nanoparticles. *J. Phys. Chem. B* 2001, 105 8797-8800
- [19] Simon, U., Charge Transport in Nanoparticle Arrangements. *Adv. Mater.* 1998, 10, 1487-1492.
- [20] Quinn, A. J.; Beecher, P.; Iacopino, D.; Floyd, L.; De Marzi, G.; Shevchenko, E. V.; Weller, H.; Redmond, G., Manipulating the Charging Energy of Nanocrystal Arrays. *Small* 2005, 1, 613-618
- [21] Black, C. T.; Murray, C. B.; Sandstrom, R. L.; Sun, S., Spin-Dependent Tunneling in Self-Assembled Cobalt-Nanocrystal Superlattices. *Science* 2000, 290, 1131-1134.
- [22] van Staveren, M. P. J.; Brom, H. B.; de Jongh, L. J., Metal-cluster compounds and universal features of the hopping conductivity of solids. *Physics Reports* 1991, 208, 1-96.
- [23] Peng, D. L.; Sumiyama, K.; Konno, T. J.; Hihara, T.; Yamamuro, S., Characteristic transport properties of CoO-coated monodisperse Co cluster assemblies. *Phys. Rev. B* 1999, 60, 2093-2100.
- [24] Beverly, K. C.; Sample, J. L.; Sampaio, J. F.; Remacle, F.; Heath, J. R.; Levine, R. D., Quantum dot artificial solids: Understanding the static and dynamic role of size and packing disorder. *Proc. Natl. Acad. Sci. USA* 2002, 99, 6456-6459.
- [25] Beecher, P.; Quinn, A. J.; Shevchenko, E. V.; Weller, H.; Redmond, G., Charge Transport in Weakly Coupled CoPt₃ Nanocrystal Assemblies. *J. Phys. Chem. B* 2004, 108 9564-9567
- [26] Talapin, D. V.; Lee, J. G.; Kovalenko, M. V.; Shevchenko, E. V., Prospects of Colloidal Nanocrystals for Electronic and Optoelectronic Applications. *Chem. Rev.* 2009, 110, 389-458.
- [27] Abeles, B.; Sheng, P.; Coutts, M. D.; Arie, Y., Structural and electrical properties of granular metal films. *Adv. Phys.* 1975, 24, 407-461.
- [28] Ingold, G. L.; Nazarov, Y. V., Charge Tunneling Rates in Ultrasmall Junctions. *NATO ASI Series B* 1992, 294, 21-107.
- [29] Neugebauer, C. A.; Webb, M. B., Electrical Conduction Mechanism in Ultrathin, Evaporated Metal Films. *J. Appl. Phys.* 1962, 33, 74-82.
- [30] Giaever, I.; Zeller, H. R., Superconductivity of Small Tin Particles Measured by Tunneling. *Phys. Rev. Lett.* 1968, 20, 1504-1507.
- [31] Gorter, C. J., A possible explanation of the increase of

- the electrical resistance of thin metal films at low temperatures and small field strengths. *Physica* 1951, 17, 777-780.
- [32] Lambe, J.; Jaklevic, R. C., Charge-Quantization Studies Using a Tunnel Capacitor. *Phys. Rev. Lett.* 1969, 22, 1371-1375.
- [33] Fulton, T. A.; Dolan, G. J., Observation of single-electron charging effects in small tunnel junctions. *Phys. Rev. Lett.* 1987, 59, 109-112.
- [34] Wolf, C. R.; Thonke, K.; Sauer, R., Single-electron transistors based on self-assembled silicon-on-insulator quantum dots. *Appl. Phys. Lett.* 2010, 96, 142108-3.
- [35] Sato, T.; Ahmed, H.; Brown, D.; Johnson, B. F. G., Single electron transistor using a molecularly linked gold colloidal particle chain. *J. of Appl. Phys.* 1997, 82, 696-701.
- [36] Likharev, K. K., Single-electron devices and their applications. *Proceedings of the IEEE* 1999, 87 606-632.
- [37] Markovich, G.; Collier, C. P.; Henrichs, S. E.; Remacle, F.; Levine, R. D.; Heath, J. R., Architectonic Quantum Dot Solids. *Acc. Chem. Res.* 1999, 32, 415-423.
- [38] Suvakov, M.; Tadic, B., Modeling collective charge transport in nanoparticle assemblies. *J. Phys. Cond. Matter* 2010, 22, 163201.
- [39] Parthasarathy, R.; Lin, X. M.; Elteto, K.; Rosenbaum, T. F.; Jaeger, H. M., Percolating through Networks of Random Thresholds: Finite Temperature Electron Tunneling in Metal Nanocrystal Arrays. *Phys. Rev. Lett.* 2004, 92, 076801.
- [40] Parthasarathy, R.; Lin, X. M.; Jaeger, H. M., Electronic Transport in Metal Nanocrystal Arrays: The Effect of Structural Disorder on Scaling Behavior. *Phys. Rev. Lett.* 2001, 87, 186807.
- [41] Shevchenko, E. V.; Talapin, D. V.; Rogach, A. L.; Kornowski, A.; Haase, M.; Weller, H., Colloidal Synthesis and Self-Assembly of CoPt₃ Nanocrystals. *J. Am. Chem. Soc.* 2002, 124, 11480-11485
- [42] Jing, P.; Zheng, J.; Zeng, Q.; Zhang, Y.; Liu, X.; Liu, X.; Kong, X.; Zhao, J., Shell-dependent electroluminescence from colloidal CdSe quantum dots in multilayer light-emitting diodes. *J. Appl. Phys.* 2009, 105, 044313.
- [43] Urban, J. J.; Talapin, D. V.; Shevchenko, E. V.; Kagan, C. R.; Murray, C. B., Synergism in binary nanocrystal superlattices leads to enhanced p-type conductivity in self-assembled PbTe/Ag₂Te thin films. *Nat. Mater.* 2007, 6, 115-121.
- [44] George, S. M., Atomic Layer Deposition: An Overview. *Chem. Rev.* 2009, 110, 111-131.
- [45] Puurunen, R. L., Surface chemistry of atomic layer deposition: A case study for the trimethylaluminum/water process. *J. Appl. Phys.* 2005, 97, 121301-52.
- [46] Ancona, M. G.; Kruppa, W.; Rendell, R. W.; Snow, A. W.; Park, D.; Boos, J. B., Coulomb blockade in single-layer Au nanocluster films. *Phys. Rev. B* 2001, 64, 033408.
- [47] Beecher, P.; Shevchenko, E. V.; Weller, H.; Quinn, A. J.; Redmond, G., Magnetic-Field-Directed Growth of CoPt₃ Nanocrystal Microwires. *Adv. Mater.* 2005, 17 1080-1083
- [48] Tan, R. P.; Carrey, J.; Desvaux, C.; Lacroix, L. M.; Renaud, P.; Chaudret, B.; Respaud, M., Magnetoresistance and collective Coulomb blockade in superlattices of ferromagnetic CoFe nanoparticles. *Phys. Rev. B* 2009, 79, 174428.
- [49] Blunt, M. O.; Suvakov, M.; Pulizzi, F.; Martin, C. P.; Pauliac-Vaujour, E.; Stannard, A.; Rushforth, A. W.; Tadic, B.; Moriarty, P., Charge Transport in Cellular Nanoparticle Networks: Meandering through Nanoscale Mazes. *Nano Letters* 2007, 7, 855-860.
- [50] Joung, D.; Zhai, L.; Khondaker, S. I., Coulomb blockade and hopping conduction in graphene quantum dots array. *Phys. Rev. B* 2011, 83, 115323.

Supporting Information

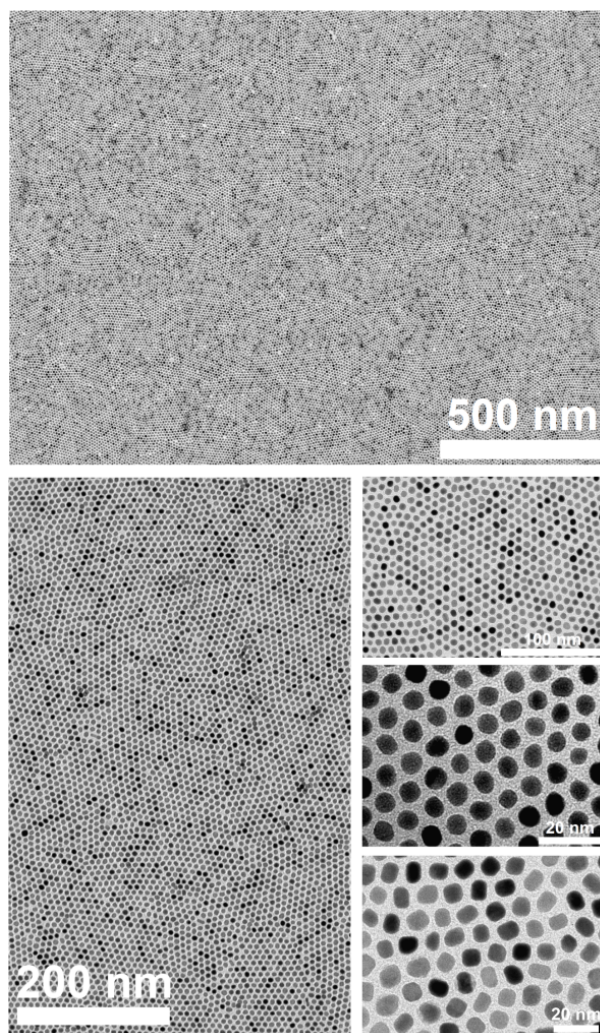


FIG. S 1: TEM zoom series of a Langmuir-Blodgett film using spherical nanoparticles. In the lower right corner a film using larger, cubic nanoparticles is shown.

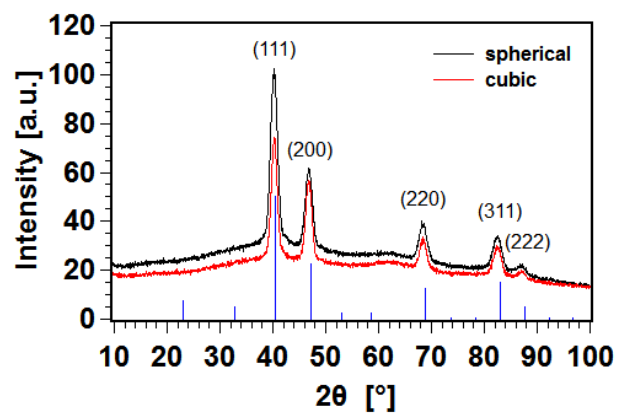


FIG. S 2: XRD of spherical and cubic nanoparticles with reference reflexes of cubic CoPt₃.

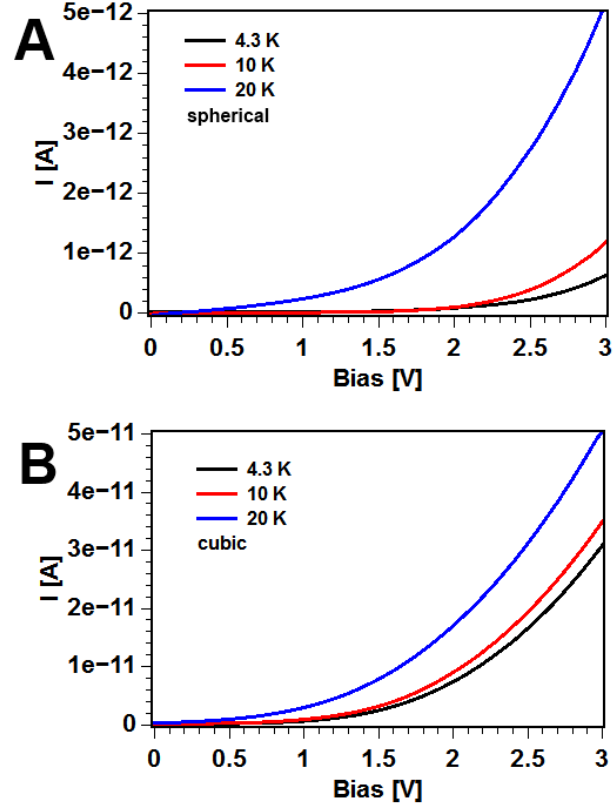


FIG. S 3: 2-point measurements: Lateral current I_D as a function of the bias V_{DS} and temperature using (A) spherical and (B) cubic nanoparticles. Both nanoparticle films are covered with a 77 nm Al_2O_3 layer. The back gate voltage is set to 0 V. The top gate is floating.

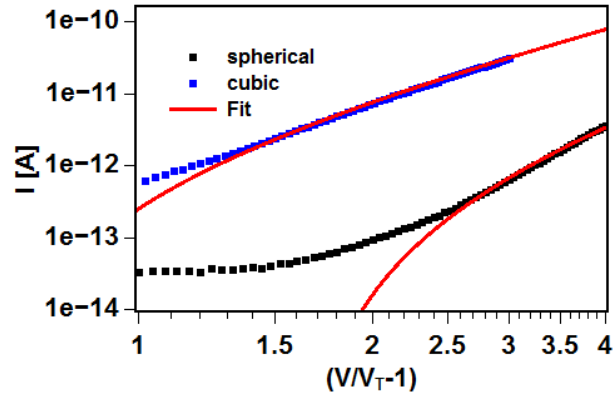


FIG. S 4: I_D - V_{DS} curves of spherical and cubic nanoparticles at 4.3 K with the Middleton-fit.

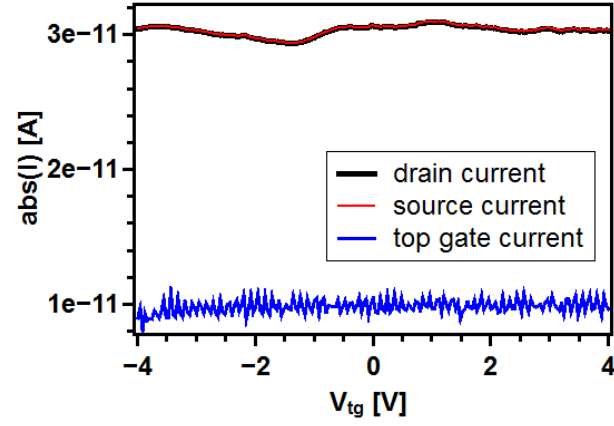


FIG. S 5: Exemplarily the lateral current I_D as a function of the applied top-gate voltage V_{tg} is shown for cubic nanoparticles at a bias of -3 V. The absolute value of the source current and the drain current perfectly overlap. The "leakage current" to the top gate is much lower than the signal currents. There is no sign of the signal in the top gate current, and the gate current is in the noise.

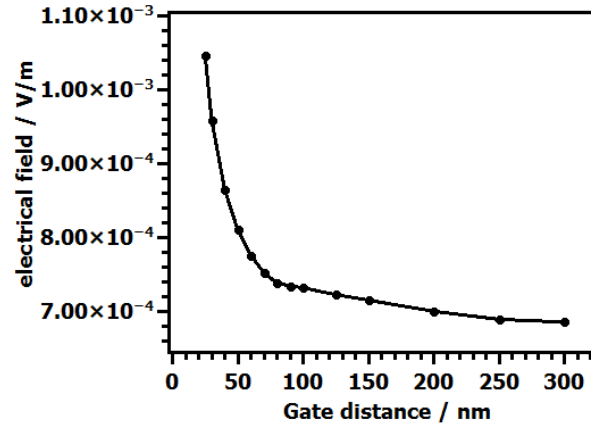


FIG. S 6: Highest field along the path through the nanoparticles under the top gate as function of top gate distance to the SiO_2 substrate.